A NEW DIRECTIONAL, LOW-REDUNDANCY, COMPLEX-WAVELET TRANSFORM

Felix C. A. Fernandes[r], Rutger L. van Spaendonck[d] and C. Sidney Burrus[r]

[r] Department of Electrical and Computer Engineering, Rice University,Houston, TX 77251-1892, USA
[d] Applied Earth Sciences, Delft University of Technology, Delft, Netherlands

ABSTRACT

Shift variance and poor directional selectivity, two major disadvantages of the discrete wavelet transform, have previously been circumvented either by using highly redundant, non-separable wavelet transforms or by using restrictive designs to obtain a pair of wavelet trees with a transform-domain redundancy of 4.0 in 2D. In this paper, we demonstrate that excellent shift-invariance properties and directional selectivity may be obtained with a transform-domain redundancy of only 2.67 in 2D. We achieve this by projecting the wavelet coefficients from Selesnick's almost shift-invariant, double-density wavelet transform so as to separate approximately the positive and negative frequencies, thereby increasing directionality. Subsequent decimation and a novel inverse projection maintain the low redundancy while ensuring perfect reconstruction. Although our transform generates complex-valued coefficients allowing processing capabilities that are impossible with real-valued coefficients, it may be implemented with a fast algorithm that uses only real arithmetic. To demonstrate the efficacy of our new transform, we show that it achieves state-of-the-art performance in a seismic image-processing application.

1. INTRODUCTION

Although the Discrete Wavelet Transform (DWT) is a powerful signal-processing tool, it has two serious disadvantages: shift variance and poor directional selectivity. The DWT is shift variant because transform coefficients behave unpredictably under shifts of the input signal, a problem that has been treated by introducing large amounts of redundancy into the transform to make it shift invariant. The 2D DWT has poor directional selectivity because it can only distinguish between three different spatial-feature orientations. Non-separable transforms [1, 2] can provide shift invariance and/or directional selectivity but these involve complicated design problems, are computationally expensive and may not be multiscale. Kingsbury's Dual-Tree Wavelet Transform (DTWT) [3] is a separable, multiscale transform with impressive shift invariance and directional selectivity. Its complex-valued transform coefficients allow for processing capabilities that are impossible with real-valued coefficients; however, these complex-valued coefficients create a transform-domain redundancy of 4.0 in 2D.

Recently Selesnick et al. [4] proposed the Double-Density Wavelet Transform (DDWT), an almost shift-invariant, multiscale transform with a low transform-domain redundancy of 2.67 in 2D. The DDWT produces real-valued coefficients and does not enjoy the superior directionality of the DTWT. In this paper, we perform non-redundant post projection [5] on DDWT coefficients, thereby obtaining a Complex, directional Double-Density Wavelet Transform (CDDWT). The CDDWT not only retains the low-redundancy (2.67) and shift-insensitivity of the DDWT, but also enjoys the superior directional selectivity and complex-valued transform coefficients of the DTWT. In addition, the CDDWT may be implemented in a perfect reconstruction framework using fast real-arithmetic algorithms.

The authors gratefully acknowledge the assistance of Prof. Ivan Selesnick. This work was supported by DARPA, Texas Instruments, the Dutch Science Foundation's NEESDI program and the Consortium for Computational Seismic Interpretation. Email: felixf@rice.edu

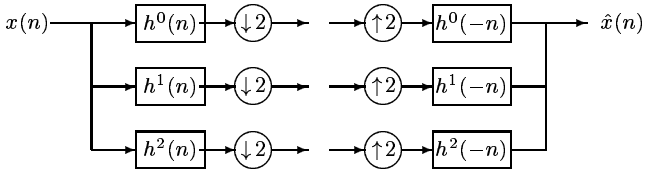

Fig. 1. *The DDWT analysis and synthesis filter bank.*

2. THE DOUBLE-DENSITY WAVELET TRANSFORM

Selesnick et al. [4] introduce the DDWT as the tight-frame equivalent of Daubechies orthonormal wavelet transform; the wavelet filters are of minimal length and satisfy certain important polynomial properties in an oversampled framework. Because the DDWT, at each scale, has twice as many wavelets as the DWT, it achieves lower shift sensitivity than the DWT. The DDWT is implemented on discrete-time signals using the oversampled analysis and synthesis filter bank shown in Figure 1. The frequency responses for the analysis-bank filters are as shown in Figure 2, for a set of filters h^0, h^1, h^2 with lengths 7, 7, 5 respectively. The h^0 filter is a lowpass filter, while the h^1 and h^2 filters are highpass filters with similar frequency magnitude responses. An iterated oversampled filter bank is created by the usual iteration on the lowpass branches of the analysis and synthesis banks. Selesnick et al. show that the above DDWT implementation corresponds to a multiresolution analysis with a single scaling function ϕ and two wavelets ψ^1, ψ^2 as shown in Figure 2. Observe that the wavelets approximately satisfy the "half-delay" property $\psi^1(t) = \psi^2(t - \frac{1}{2})$.

The DDWT is extended to 2D by iterating the 1D oversampled filter bank on the rows and then on the columns of an image, as is usually done for separable 2D DWTs. At a given level in the iterated filter bank, this separable extension produces nine 2D subbands. To indicate the filters used along the row and column dimensions to create the nine subbands, we label the subbands $h_y^i h_x^j, \;\; i, j \in \{0, 1, 2\}$. The subscript x indicates filtering along the row dimension, while subscript y indicates filtering along the column dimension. The superscripts $0, 1, 2$ indicate the particular filter h^0, h^1, h^2 used to filter along a specified dimension to create the subband. Next, we introduce an interleaving process that operates on four disjoint subsets of the nine DDWT subbands produc-

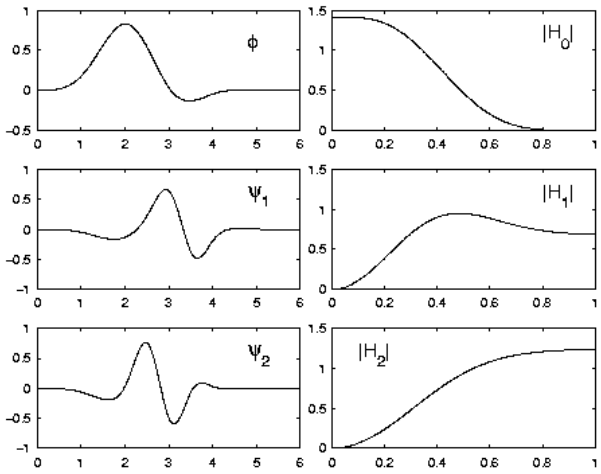

Fig. 2. *Left column: basis functions, Right column: frequency responses.*

ing four new DDWT subbands $HH_{DD}, HL_{DD}, LH_{DD}, LL_{DD}$ with frequency domain supports that are comparable to those of the HH, HL, LH, LL subbands of the 2D DWT. Subsequent processing of the interleaved DDWT subbands is then quite similar to the processing of DWT subbands.

Since h^0 is a lowpass filter while both h^1 and h^2 are highpass filters, the $h_y^2h_x^2, h_y^2h_x^1, h_y^1h_x^2, h_y^1h_x^1$ subbands each have a frequency-domain support comparable to that of the HH subband in a DWT. Although these subbands all have the same frequency domain support, the half-delay property implies that the spatial-domain supports of the wavelets corresponding to the coefficients in the columns of the $h_y^2h_x^1$ subband lie a half-integer to the right of those in the columns of the $h_y^2h_x^2$ subband. Therefore we may interleave the wavelet-coefficient columns in the $h_y^2h_x^1$ subband inbetween and to the right of the wavelet-coefficient columns in the $h_y^2h_x^2$ subband. We may also interleave the wavelet-coefficient rows in the $h_y^1h_x^2$ subband inbetween and below the wavelet-coefficient rows in the $h_y^2h_x^2$ subband. We complete the interleaving process by interleaving the wavelet-coefficient rows in the $h_y^1h_x^1$ subband inbetween and below the wavelet-coefficient rows in the $h_y^2h_x^1$ subband. We represent this interleaving process concisely in Matlab-compatible notation by

$$HH_{DD}(m,n) = \begin{cases} h_y^2h_x^2\left(\frac{m}{2},\frac{n}{2}\right), & m \text{ even}, \quad n \text{ even}, \\ h_y^2h_x^1\left(\frac{m}{2},\frac{n-1}{2}\right), & m \text{ even}, \quad n \text{ odd}, \\ h_y^1h_x^2\left(\frac{m-1}{2},\frac{n}{2}\right), & m \text{ odd}, \quad n \text{ even}, \\ h_y^1h_x^1\left(\frac{m-1}{2},\frac{n-1}{2}\right), & m \text{ odd}, \quad n \text{ odd}. \end{cases}$$

HH_{DD} is a new subband with four times as many coefficients but the same frequency-domain support as the HH subband at the same level in a DWT. A similar interleaving scheme creates the HL_{DD} (LH_{DD}) subband with the same frequency-domain support as the corresponding HL (LH) subband of the DWT, but with twice as many coefficients. We describe this interleaving scheme by

$$HL_{DD}(m,n) = \begin{cases} h_y^2h_x^0\left(\frac{m}{2},n\right), & m \text{ even}, \\ h_y^1h_x^0\left(\frac{m-1}{2},n\right), & m \text{ odd}, \end{cases}$$

$$LH_{DD}(m,n) = \begin{cases} h_y^0h_x^2\left(m,\frac{n}{2}\right), & n \text{ even}, \\ h_y^0h_x^1\left(m,\frac{n-1}{2}\right), & n \text{ odd}. \end{cases}$$

Finally, note that there is only one subband $h_y^0h_x^0$ with the same frequency domain support as the LL subband in a DWT. To maintain consistency, we label this $h_y^0h_x^0$ subband as LL_{DD}.

3. ENHANCING DDWT DIRECTIONAL SELECTIVITY

In this section, we demonstrate how separable 2D complex-coefficient filters can project the DDWT coefficients to obtain the CDDWT Fourier-plane partitioning with enhanced directional selectivity. As explained in Section 2, the Fourier-plane partitioning associated with the $HH_{DD}, HL_{DD}, LH_{DD}, LL_{DD}$ subbands of the DDWT is comparable to that of the separable real-valued DWT. Consequently, the Fourier-plane partitioning of the DDWT may be represented as in Figure 3(a). The HH_{DD} subband is associated with diagonally-oriented spatial features and concentrates its energy in the four blocks labeled HH_{DD}. The HH_{DD} blocks in the upper-left and lower-right corners indicate features with gradients at -45 degrees, while those in the upper-right and lower-left corners indicate features with gradients at $+45$ degrees. Since all four blocks are associated with one interleaved subband in the DDWT, we cannot differentiate between these two orientations. Similarly, features with gradients at $+15(+75)$ degrees and $-15(-75)$ degrees are indistinguishable from their wavelet coefficients since they are both associated with energy in the $HL_{DD}(LH_{DD})$ subband. Therefore, decoupling the positively- and negatively-oriented blocks associated with each subband of the DDWT improves directional selectivity. The CDDWT analysis filter bank in Figure 4 shows how this may be done using our non-redundant post-projection technique [5] to increase the directionality of the DDWT while preserving its low transform-domain redundancy of 2.67. The complex-coefficient filters in the block labeled "projection" have $+(-)$ superscripts to indicate that they retain positive (negative) frequencies and suppress negative (positive) frequencies. These $+(-)$ filters are 1D projection filters that project real signals onto subspaces consisting of predominantly positive (negative) frequencies in $[-\pi,\pi]$. As explained below, these projection filters enhance the directional selectivity of the DDWT transform preceding them by decoupling the DDWT subband blocks in Figure 3(a) to obtain the CDDWT subbands in Figure 3(b).

Consider the subband corresponding to the two blocks labeled LH_{DD} in Figure 3(a). If we filter this subband in the y direction (along columns) with a filter h_y^+ as shown in Figure 4, we obtain a new subband containing the two blocks labeled LH_{DD}^- and LH_{DD}^+ in Figure 3(b). We then obtain a decoupled subband LH_{DD}^+ by filtering this new subband in the x direction (along rows) with h_x^+. The other decoupled subband LH_{DD}^- is similarly obtained by row filtering with h_x^-. The decoupled subband LH_{DD}^- reveals features with gradients at -75 degrees, while the other decoupled sub-

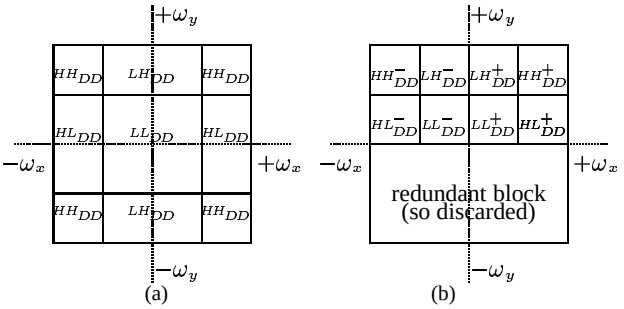

Fig. 3. ***(a)*** *DDWT Fourier-plane partitioning,* ***(b)*** *CDDWT Fourier-plane partitioning.*

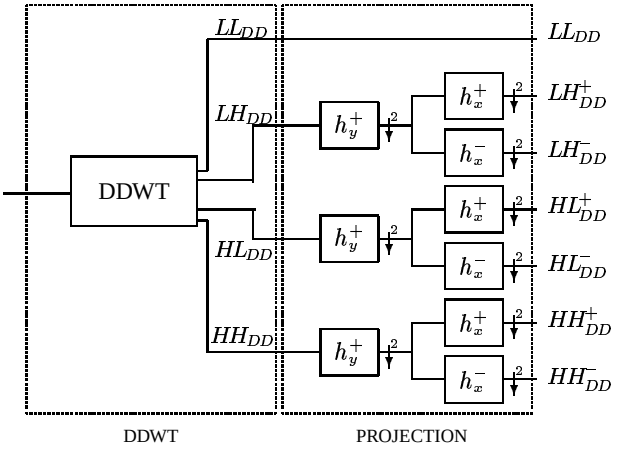

Fig. 4. *CDDWT analysis filter-bank. The y (x) subscripts indicate filtering along the columns (rows) of an image. The $+$ ($-$) superscripts indicate projection filters that attenuate negative (positive) frequencies.*

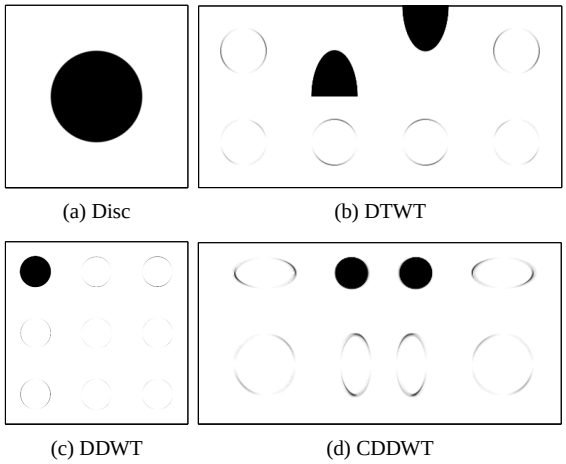

Fig. 5. ***(a)*** *Disc Image* ***(d)*** *CDDWT Clockwise from upper-rightmost block: -15, -45, -75, +75, +45, +15 degree highpass subband, upper half of lowpass subband, lower half of lowpass subband.* ***(c)*** *DDWT: From top to bottom, left to right: $h_y^0h_x^0, h_y^1h_x^0, h_y^2h_x^0, h_y^0h_x^1, h_y^1h_x^1, h_y^1h_x^2, h_y^0h_x^2, h_y^2h_x^1, h_y^2h_x^2$* ***(d)*** *CDDWT: Clockwise from upper-rightmost block: -15, -45, -75, +75, +45, +15 degree highpass subbands, -45, +45 degree lowpass subbands.*

band LH^{1+}_{DD} reveals features with gradients at +75 degrees. Likewise, the subbands labeled $HL^+_{DD}, HL_{DD}-, HH^+_{DD}, HH^-_{DD}$ indicate features with gradients at +15, -15, +45, -45 degrees respectively, giving a total of 6 directional subbands at each scale. Although not shown in Figure 4, we can also use the projection filters to decouple the lowpass subband LL_{DD} into LL^-_{DD} and LL^+_{DD} subbands that discriminate between low-scale features oriented at -45 and +45 degrees.

Obtaining perfect reconstruction for the CDDWT requires the design of a synthesis filter bank that inverts the analysis filter bank in Figure 4. The DDWT is easily inverted by a synthesis filter bank that performs the inverse DDWT. However, inversion of the projection block is a non-trivial problem due to the presence of the decimators ensuring that no additional redundancy is introduced by the projection block. In [5], we solved this problem using fast real-arithmetic structures for the implementation of the projection block and its inverse.

4. RESULTS AND CONCLUSIONS

To compare the directional selectivity of various different transforms, we used the disc image displayed in Figure 5(a). Figure 5(c) shows the nine subbands $h_y^i h_x^j, \quad i,j \in \{0,1,2\}$ from the single-level DDWT of the disc image. Observe that directional information is not readily available in this transform. Figure 5 (b) shows the single-level DTWT of the disc image. Due to its large size, the lowpass subband has been displayed in halves. Figure 5 (d) presents the single-level CDDWT obtained using the filter-bank structure of Figure 4. Note that the interleaving process creates rectangular $LH^+_{DD}, LH^-_{DD}, HL^+_{DD}, HL^-_{DD}$ subbands in the CDDWT; although the disc appears elliptical in these subbands, the CDDWT directionality is unaffected. While the DTWT and the CDDWT each provide six highpass directional subbands at each scale, the DTWT transform-domain redundancy is 4.0, whereas that of the CDDWT is only 2.67.

Next, we used the following experiment to compare the shift sensitivity of the CDDWT with that of other multiscale tranforms. We retained the lowest scale $HH, HH_{DD}, HH^+, HH^+_{DD}$ subbands of the disc image (Figure 5(a)) using 3-level DWT, DDWT, DTWT and CDDWT transforms respectively, and zeroed out all other subbands. Figures 6(a) and 6(c) show the reconstruction of the disc image from the lowest scale HH^+_{DD} and HH subbands of the 3-level CDDWT and DWT respectively. The input disc image was then shifted one pixel rightwards and downwards and the same reconstruction was performed using each of the above transforms. Figures 6(b) and 6(d) show the reconstruction of the shifted-disc image from the level-3 CDDWT HH^+_{DD} subband and the level-3 DWT HH subband respectively. Observe that the pre-shift and post-shift DWT reconstructions appear significantly different, whereas there are very minor differences in the CDDWT reconstructions. This indicates that the HH^+_{DD} CDDWT subband is much less shift sensitive than the HH DWT subband. For each transform, we then spatially translated the post-shifted reconstruction so that its center coincided with that of the pre-shifted reconstruction. Next we computed the root mean square error between the translated post-shifted reconstruction and the pre-shifted reconstruction. This was repeated for shifts ranging from one to eight pixels. The bar graph in Figure 7 summarizes the results. The DWT HH subband is the most shift-sensitive, while the DDWT HH_{DD} and DTWT HH^+ subbands are the least shift-sensitive. The CDDWT HH^+_{DD} subband is much less shift-sensitive than the DWT HH subband and also enjoys both the low-redundancy (2.67) of the DDWT as well as the enhanced directionality of the DTWT.

Finally we compared the performance of the CDDWT to that of other directional transforms in a seismic image-processing application. Seismic imagery of the earth's subsurface plays a critical role in all aspects of oil exploration. Local signal attributes aid the interpretation of seismic data, elucidating its salient characteristics. A particularly useful attribute is the local angle (dip) of the reflecting surface. Angle representations enable 3D interpretation of *structures* by indicating steep uphill-dipping reflections with high intensity and steep downward-dipping reflections with low intensity. To compare angle representations generated for a seismic cross-section with substantial angle variations (Figure 8(a)), we used a two-stage method [5] that exploits a direc-

tional multiscale transform. Although, the Complex-Steerable-Pyramid (CSP) [1] angle representation in Figure 8(b) provides an accurate and smooth representation of the local angles in the seismic section, it has a transform-domain redundancy of 14.0. On the other hand, besides appearing equally informative as the CSP result (Figure 8(b)), the CDDWT angle-representation in Figure 8(d) has a higher spatial resolution and a transform-domain redundancy of only 2.67. For comparison, in Figure 8(c) we present the somewhat noisier angle-representation generated from the non-redundant post-projection transform [5] with no transform-domain redundancy.

In conclusion, we emphasize that the CDDWT retains the shift-insensitivity and low transform-domain redundancy (2.67) of the DDWT while offering directionality comparable to that of the dual-tree wavelet transform which has higher transform-domain redundancy (4.0). In addition, the complex-valued CDDWT transform coefficients allow for interesting processing capabilities that are impossible with the real-valued coefficients of the DWT or DDWT. All these properties together with its fast, real-arithmetic implementation ensure that the CDDWT will be a powerful tool for seismic- and image-processing applications.

5. REFERENCES

[1] E. P. Simoncelli, W. T. Freeman, E. H. Adelson, and D. J. Heeger, "Shiftable multi-scale transforms," *IEEE Trans. Inform. Theory*, vol. 38, no. 2, pp. 587–607, Mar. 1992.

[2] R. H. Bamberger and M. J. T. Smith, "A filter bank for the directional decomposition of images: Theory and design," *IEEE Transactions on Signal Processing*, vol. 40, no. 4, pp. 882–893, Apr. 1992.

[3] N. Kingsbury, "Image processing with complex wavelets," *Phil. Trans. R. Soc. Lond.*, Sept. 1999.

[4] I. W. Selesnick and L. Sendur, "Iterated oversampled filter banks and wavelet frames," in *Wavelet Applications VII, Proceedings of SPIE*, 2000.

[5] F. C. A. Fernandes, R. van Spaendonck, M. Coates, and C. S. Burrus, "Directional complex-wavelet processing," in *Wavelet Applications VII, Proceedings of SPIE*, 2000.

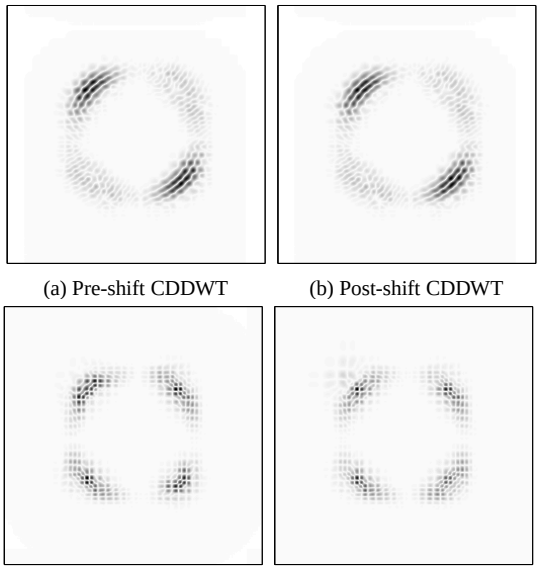

(a) Pre-shift CDDWT (b) Post-shift CDDWT

(c) Pre-shift DWT (d) Post-shift DWT

Fig. 6. *Single-subband disc reconstructions comparing shift-sensitivity*

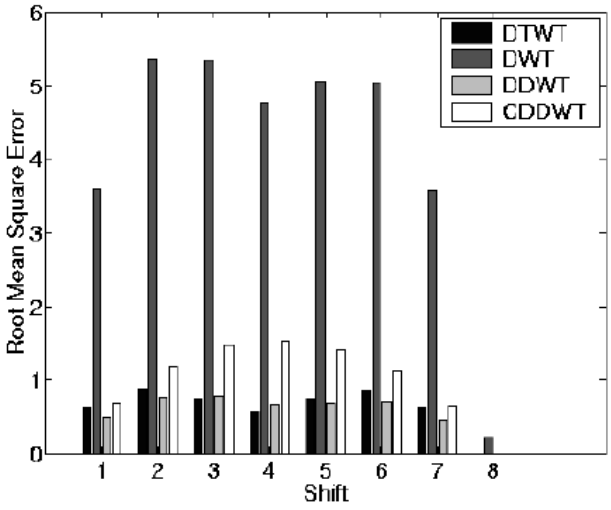

Fig. 7. *Bar graph comparing RMSE vs. Shift for various transforms.*

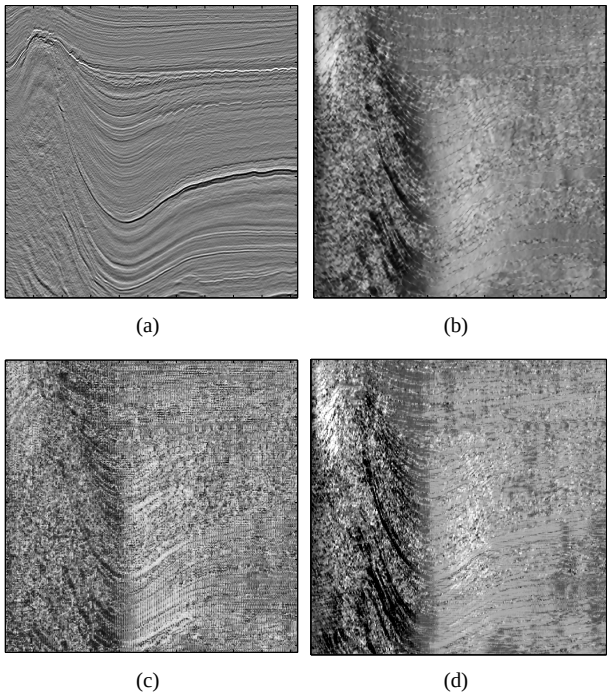

(a) (b)

(c) (d)

Fig. 8. ***(a)*** *Seismic cross-section,* ***(b)*** *CSP angle-analysis results,* ***(c)*** *Angle-analysis results using the non-redundant post-projection transform,* ***(d)*** *CDDWT angle-analysis results. In (b),(c) and (d) intensity represents angle, black (-90 degrees) through white (+90 degrees).*